# Correlation between symmetry energy and effective $k$-mass splitting with an improved isospin- and momentum-dependent interaction

Jun Su,[1,*] Long Zhu,[1] Ching-Yuan Huang,[1,2] Wen-Jie Xie,[3,4] and Feng-Shou Zhang[5,6,7]

[1]*Sino-French Institute of Nuclear Engineering and Technology, Sun Yat-sen University, Zhuhai 519082, China*

[2]*School of General Education, Northwestern Polytechnic University, 47671 Westinghouse Drive, Fremont, California 94539, USA*

[3]*Department of Physics, Yuncheng University, Yuncheng 044000, China*

[4]*Institute of Modern Physics, Chinese Academy of Sciences, Lanzhou 730000, China*

[5]*The Key Laboratory of Beam Technology and Material Modification of Ministry of Education, College of Nuclear Science and Technology, Beijing Normal University, Beijing 100875, China*

[6]*Beijing Radiation Center, Beijing 100875, China*

[7]*Center of Theoretical Nuclear Physics, National Laboratory of Heavy Ion Accelerator of Lanzhou, Lanzhou 730000, China*

(Received 30 June 2016; published 29 September 2016)

The isospin- and momentum-dependent interaction using the isospin-dependent quantum molecular dynamics model is improved. The momentum dependence of the interaction is fitted to the optical potentials extracted with proton-nucleus scattering data, while the isospin dependence is adjusted based on the current constraints on the symmetry energy and its density slope at normal density. The resulting parameters of the interaction are used to calculate the effective masses characterized by the nonlocality of the nuclear potential in the spatial coordinates (the so-called effective $k$ masses). It is found that this parametrization can reproduce the effective $k$ masses calculated by the Dirac-Brueckner-Hartree-Fock model. The current constraints on the total symmetry energy can accommodate a wide-range adjustment of the local symmetry energy and effective $k$-mass splitting. Four groups of parameters, which provide different density dependences of symmetry energy and effective $k$-mass splitting, are applied to investigate the isospin diffusion and neutron to proton double ratios in collisions involving $^{124}$Sn and $^{112}$Sn nuclei at 50 and 120 MeV/nucleon. Calculations confirm the sensitivity of symmetry energy to the isospin diffusion, but indicate the synchronous effects of symmetry energy and effective $k$-mass splitting on the double ratios.

DOI: 10.1103/PhysRevC.94.034619

## I. INTRODUCTION

The residual strong interactions between nucleons are of fundamental importance in understanding the nature of asymmetric nuclear objects including supernovae, neutron stars, as well as nuclei [1–4]. However, there still exist large uncertainties in our current knowledge. Generally speaking, the residual strong interactions can be described by the nuclear potential energy $U(\rho,\mathbf{p},\delta)$ for a nucleon with momentum $\mathbf{p}$ in asymmetric nuclear matter with density $\rho$ and isospin asymmetry $\delta = (\rho_n - \rho_p)/(\rho_n + \rho_p)$. In recent decades, heavy-ion collisions (HICs) have been applied to study the density and isospin dependence of the nuclear potential energy. Much progress has been made especially at normal and subnormal densities, but many interesting issues remain to be resolved [5–7]. On the other hand, the significance of the momentum-dependent potential, especially its difference between neutrons and protons, has been emphasized to understand the dynamics of HICs [8–10].

Decades ago the momentum dependent potential was predicted from microscopic *ab initio* calculations, such as the Dirac-Brueckner-Hartree-Fock (DBHF) model [11–15], the Skyrme-Hartree-Fock model [16], and the relativistic mean-field (RMF) model [17]. In the transport models, the momentum-dependent potential is always parametrized from the proton-nucleus optical potential in the energy range 10 MeV $< E_{\rm kin} <$ 1 GeV [18–23]. In addition, the concept of nonrelativistic effective mass $m^*$ is used to parametrize the the nonlocality of the single-particle potential [24,25]. The so-called effective $k$ mass and effective $E$ mass are also introduced in order to clearly separate the nonlocality of the single-particle potential both in space and in time [11,12]. Generally speaking the nucleon effective mass in symmetric nuclear medium is well determined as $m^*/m = 0.7 \pm 0.05$, at normal density and Fermi momentum [5–7]. However, the splitting of the effective masses between neutrons and protons in asymmetric nuclear medium has been a long-standing and controversial issue [26–28].

The data from HICs have been applied to constrain the symmetry energy and effective mass splitting [29–33]. However, most of the observables, known to be sensitive to the effective mass splitting, are also sensitive to the local symmetry energy. For example, the isospin diffusion and neutron-to-proton double ratio at the Fermi-dominated incident energies have been analyzed to constrain the density dependence of the symmetry energy [34,35]. Nevertheless, it has been found that the momentum-dependent potential affects the sensitivity of the isospin diffusion to the density dependence of the symmetry energy [36]. Besides, it has also been shown that the effective mass splitting obviously affects the neutron-to-proton double ratio from heavy-ion reactions around 50–300 MeV/nucleon [32,33,37]. On the other hand, the effect of the kinetic symmetry energy on the double ratios

*Corresponding author: sujun3@mail.sysu.edu.cn

 

has also been found [38,39]. The challenge is that the nuclear symmetry energy and the effective mass splitting are explicitly related to each other [40–42].

In this article, in order to study the correlation between symmetry energy and effective $k$-mass splitting, we improve the isospin- and momentum-dependent nuclear potentials according to the current constraints on the optical potentials and the symmetry energy. The relative effects of the symmetry energy and the effective $k$-mass splitting on the isospin diffusion and the double ratio are investigated within the framework of the isospin-dependent quantum molecular dynamics (IQMD) model in combination with the statistical decay code GEMINI.

## II. IMPROVED ISOSPIN- AND MOMENTUM-DEPENDENT INTERACTION

### A. Parametrization of nuclear interaction

The nuclear interaction can be described by the potential energy density of the asymmetric nuclear matter with density $\rho$ and asymmetry $\delta$:

$$\begin{aligned} V(\rho,\delta) &= \frac{\alpha}{2}\frac{\rho^2}{\rho_0} + \frac{\beta}{\gamma+1}\frac{\rho^{\gamma+1}}{\rho_0^{\gamma}} + \frac{C_{\rm sp}}{2}\left(\frac{\rho}{\rho_0}\right)^{\gamma_i}\rho\delta^2 \\ &+ \sum_{\tau}(1+x)\iint v(\mathbf{p},\mathbf{p}')f_\tau(\mathbf{r},\mathbf{p})f_\tau(\mathbf{r},\mathbf{p}')d\mathbf{p}d\mathbf{p}' \\ &+ \sum_{\tau}(1-x)\iint v(\mathbf{p},\mathbf{p}')f_\tau(\mathbf{r},\mathbf{p})f_{-\tau}(\mathbf{r},\mathbf{p}')d\mathbf{p}d\mathbf{p}', \\ v(\mathbf{p},\mathbf{p}') &= \frac{C_m/\rho_0}{1+(\mathbf{p}-\mathbf{p}')^2/\Lambda^2}, \end{aligned} \tag{1}$$

where $\rho_0$ is the normal density, $\mathbf{p}$ and $\mathbf{p}'$ are the momenta of the nucleon, and $f_\tau(\mathbf{r},\mathbf{p})$ is the phase-space density, with $\tau = 1/2$ for neutrons and $\tau = -1/2$ for protons. For infinite nuclear matter at zero temperature, the phase-space density can be approximated as a step function, $f_\tau(\mathbf{r},\mathbf{p}) = \frac{3}{8\pi p_{F\tau}^3}\Theta(p_{F\tau}-p)$. The parameters $\alpha$, $\beta$, $\gamma$, $C_{\rm sp}$, $\gamma_i$, $x$, $C_m$, and $\Lambda$ are temperature independent. In Eq. (1), the first and second terms refer to the local two-body and three-body interactions, which are widely used in the transport models [43]. The form of the local symmetric potential, shown as the third term in Eq. (1), was proposed by Tsang *et al.* [34]. The fourth and fifth terms refer to the momentum dependent interactions. In this work, we choose the form proposed by Welke *et al.* [44].

The energy per nucleon of the asymmetric nuclear matter at zero temperature is the summation of kinetic energy and potential energy:

$$\begin{aligned} E(\rho,\delta) &= \frac{3}{5}\frac{p_{Fn}^2}{2m}\frac{\rho_n}{\rho} + \frac{3}{5}\frac{p_{Fp}^2}{2m}\frac{\rho_p}{\rho} + \frac{V(\rho,\delta)}{\rho}, \\ p_{Fn} &= \hbar c\left(\frac{3\pi^2\rho}{2}\right)^{1/3}(1+\delta)^{1/3}, \\ p_{Fp} &= \hbar c\left(\frac{3\pi^2\rho}{2}\right)^{1/3}(1-\delta)^{1/3}, \end{aligned} \tag{2}$$

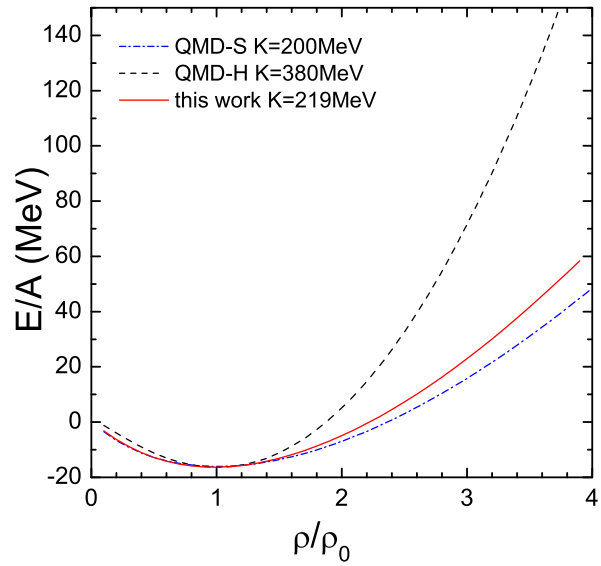


FIG. 1. Energy per nucleon as a function of density in symmetric nuclear matter at zero temperature.

where $p_{Fn}$ and $p_{Fp}$ are the Fermi momenta of neutrons and protons.

The corresponding single-particle potentials of neutron and proton with momentum $\mathbf{p}$ in asymmetric nuclear matter with density $\rho$ and asymmetry $\delta$ can be calculated as

$$\begin{aligned} U_\tau(\rho,\delta,\mathbf{p}) &= \frac{\partial V(\rho,\delta)}{\partial\rho_\tau} = \alpha\frac{\rho}{\rho_0} + \beta\frac{\rho^\gamma}{\rho_0^\gamma} \\ &+ \frac{C_{\rm sp}(\gamma_i+1)}{2}\frac{\rho^{\gamma_i}}{\rho_0^{\gamma_i}}\delta^2 + \frac{|\tau|}{\tau}\frac{C_{\rm sp}}{2}\frac{\rho^{\gamma_i+1}}{\rho_0^{\gamma_i}}2\delta \\ &+ 2(1+x)\int v(\mathbf{p},\mathbf{p}')f_\tau(\mathbf{r},\mathbf{p}')d\mathbf{p}' \\ &+ 2(1-x)\int v(\mathbf{p},\mathbf{p}')f_{-\tau}(\mathbf{r},\mathbf{p}')d\mathbf{p}'. \end{aligned} \tag{3}$$

### B. EOS of symmetric nuclear matter

The parameters $\alpha$, $\beta$, $\gamma$, $C_m$, and $\Lambda$ can be fitted by the equation of state (EOS) of symmetric nuclear matter at zero temperature. Considering the empirical constraints of the binding energy, the pressure $P$, the incompressibility $K$, and the momentum dependence of the single-particle potentials at normal density $\rho_0 = 0.16$ fm$^{-3}$, we obtain the parameters $\alpha = -75.86$ MeV, $\beta = 166.43$ MeV, $\gamma = 1.226$, $C_m = -88.21$ MeV, and $\Lambda = 664.86$ MeV $c$. The corresponding energy per nucleon as a function of density is shown in Fig. 1. The soft EOS ($K = 200$ MeV) and hard EOS ($K = 380$ MeV), which have been widely used in QMD models [43], are also shown in the figure. The parameters used in this work provide the binding energy $E(\rho_0,0) = -16.3$ MeV. The incompressibility is 219 MeV, in the middle of the soft and hard EOS's.

The corresponding energy dependence of single-particle potentials in symmetric nuclear matter at $0.5\rho_0$, $\rho_0$, and $1.5\rho_0$ is show as dashed curves in Fig. 2. For comparison,

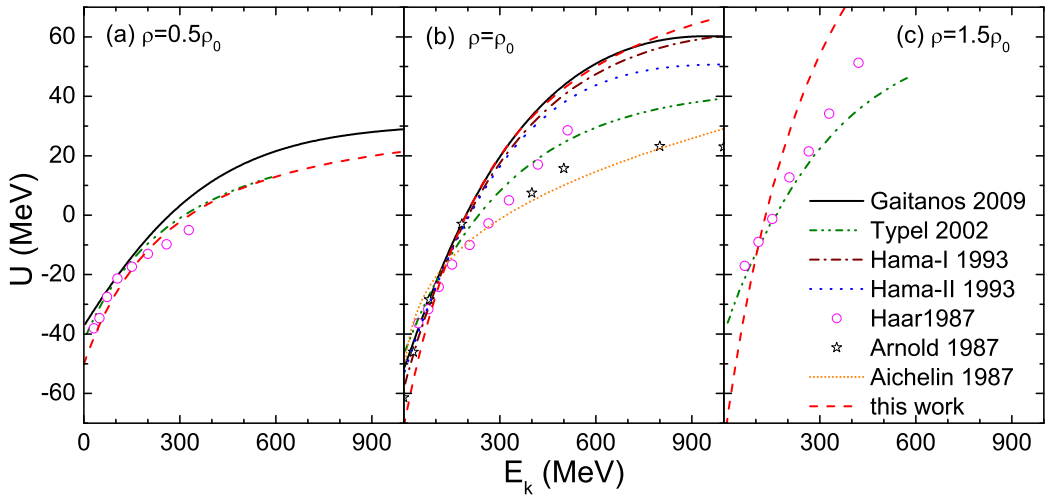


FIG. 2. Energy dependence of single particle potentials in symmetric nuclear matter at (a) $0.5\rho_0$, (b) $\rho_0$, and (c) $1.5\rho_0$. For comparison, the figures also show the real parts of the optical potential calculated using the nonlinear derivative model by Gaitanos *et al.* (solid curves) [45], calculated using the relativistic mean field model by Typel *et al.* (dash-dot-dotted curves) [46], phenomenologically fitted from the proton-nucleus scattering data by Hama *et al.* (dash-dotted curve for one fitting and dotted curve for another fitting) [19,20], calculated with the Dirac-Brueckner approach by ter Haar and Malfliet (open circles) [47], and phenomenologically fitted the proton-nucleus scattering data by Arnold *et al.* (open stars) [18].

the figures also show the real parts of the optical potential calculated using the nonlinear derivative (NLD) model by Gaitanos *et al.* (solid curves) [45], the RMF model by Typel *et al.* (dash-dot-dotted curves) [46], the Dirac-Brueckner (DB) approach by ter Haar and Malfliet (open circles) [47], as well the phenomenologically fitted proton-nucleus scattering data by Hama *et al.* (dash-dotted curve for one fitting and dotted curve for another fitting) [19,20] and the proton-nucleus scattering data by Arnold *et al.* (open stars) [18].

Figure 2(a) shows the case at $0.5\rho_0$. It can be seen that the potentials at energy $E_k = 100$ MeV proposed by different models are similar. The divergence occurs at high energies. At 600 MeV, the divergence between calculations using the NLD model and the RMF model is about 10 MeV. At low energies ($0 < E_k < 300$ MeV), our parametrization reproduces the energy dependence of the optical potential by the DB approach. At energies between 300 and 600 MeV, it is close to that by the NLD model.

Figure 2(b) shows the case at normal density $\rho_0$. Near energy 100 MeV different models propose similar values of potential, while at high energy the divergence is considerable. At energy 1000 MeV, the minimum (23 MeV) is proposed by the empirical constraints from the proton-nucleus scattering data, and the maximum (60 MeV) is proposed by the NLD model. Their divergence is about 37 MeV. In fact, from the real part of optical potentials predicted by Arnold *et al.*, the "ln-type" parametrization of momentum-dependent potentials has been fitted and applied in the QMD model [22]. This parametrization, $-54 + 1.57\ln^2(0.0005p^2 + 1)$, is shown as the densely dotted curve. Hama *et al.* developed the empirical constraints of the optical potentials by a more extensive analysis and more abundant data [19,20]. Two fits in the phenomenological parametrization were obtained, which are shown as the dash-dotted curve and dotted curve in Fig. 2(b). One can see that the "ln-type" momentum dependent potentials deviate obviously from the optical potentials proposed by Hama *et al.* In this work, the energy dependence of single-particle potentials in symmetric nuclear matter is parametrized by fitting the empirical constraints by Hama *et al.* It can be seen that our parametrization (dashed curve) agrees well with the empirical constraints by Hama *et al.* except at Fermi energies and near 1000 MeV. It is noted there are small deviations at Fermi energies and near 1000 MeV, because some other properties of the EOS have been taken into account.

In Fig. 2 (c), the single-particle potentials in symmetric nuclear matter at $1.5\rho_0$ are compared to the real part of the optical potential calculated by RMF and DB models. We also find similar values near 100 MeV. However, with increasing energies, the value in this work increases more rapidly than those by RMF and DB models.

Besides the magnitude of the single-particle potential, its gradient of momentum, i.e., $dU/dp$, is an important characteristic. It is usually described by a common concept of nonrelativistic effective mass $m^*$. The effective mass of a nucleon in the nuclear medium is defined as [12]

$$m_\tau^* = p\left(\frac{dE_\tau}{dp}\right)^{-1}. \tag{4}$$

The approximation $E_\tau = p^2/2m_\tau + U_\tau$ is considered, yielding the following expression for the effective mass:

$$m_\tau^* = \left[\frac{1}{m_\tau} + \frac{\partial U_\tau}{p\partial p}\right]^{-1}. \tag{5}$$

Actually, the origins of the effective mass include the nonlocality in space (resulting in $k$ mass) and nonlocality in time (resulting in $E$ mass) [11,12]. The effective mass defined by Eq. (5) contains both, but Eqs. (3) and (5) yield the effective $k$ mass. Only the nonlocality in space is considered in Eq. (3). We calculate the effective $k$ masses at normal density as a function

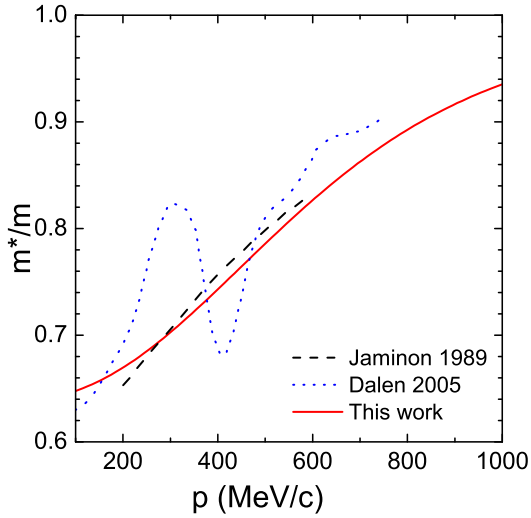


FIG. 3. Effective masses as a function of momentum in symmetric nuclear matter at normal density. The solid line shows our calculations. The dotted line displays the calculation by DBHF model considering both nonlocality in space and nonlocality in time [12]. The dashed line displays the calculation by DBHF model without considering nonlocality in time [11].

of momentum with the parameters $C_m = -88.21$ MeV and $\Lambda = 664.86$ MeV $c$. In Fig. 3 our calculations for the symmetric nuclear matter are compared with those by the DBHF model [11,12]. The dotted line displays the calculation by the DBHF model considering nonlocalities both in space and in time. One can see a pronounced peak and valley apparently above the Fermi momentum. The dashed line displays the calculation by the DBHF model without considering the nonlocality in time. The dashed line shows a smooth increase of effective $k$ masses with increasing momenta. Our calculations, shown as the solid line, are similar to those for the dashed line displayed in the middle section of the dotted line.

It has been indicated that the nonlocality in space of the single-particle potential is mainly generated by exchanging Fock terms and the resulting $k$ mass is a smooth function of the momentum, while the nonlocality in time is generated by short-range correlations which lead to the peak and valley of the $E$ mass apparently above the Fermi momentum [3]. Obviously, the potential shown as Eq. (3) does not include the short-range correlations of the nuclear interaction. However, in transport model simulations of nuclear reactions, the short-range correlations are represented by means of Pauli-suppressed two-nucleon collisions [48].

### C. Symmetry energies and effective $k$-mass splittings

The parameter $x$ in Eq. (3) is introduced to provide neutron-proton effective $k$-mass splitting. Since not only the magnitude but also the sign of the effective $k$-mass splitting have been a controversial issue, the parameter $x$ is set as $-0.4$ and 0.4, instead of being fitted by the empirical constraints. As shown in Figs. 4(a) and 4(b), $x = -0.4$ provides $m_n^* > m_p^*$ in neutron-rich nuclear matter, while $x = 0.4$ provides $m_n^* < m_p^*$. It will

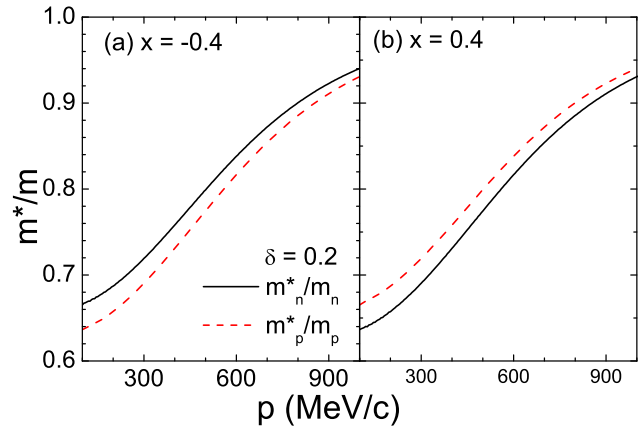


FIG. 4. Effective $k$ masses of neutron and proton as a function of momentum in asymmetric nuclear matter at normal density for (a) $x = -0.4$ and (b) $x = 0.4$.

be shown in the following that the parameter $x$ affects not only the effective $k$-mass splitting but also the symmetry energy.

The parabolic approximation to the symmetry energy $E_{\rm sym}$ has been widely used [6,7]:

$$E(\rho,\delta) - E(\rho,0) = E_{\rm sym}(\rho)\delta^2 + O(\delta^4). \tag{6}$$

Considering Eqs. (1) and (2), the symmetry energy is composed of three components, i.e., the kinetic energy, the local part, and the momentum dependent part, shown as

$$\begin{aligned}
E_{\rm sym} &= E_{\rm sym}^{\rm kin} + E_{\rm sym}^{\rm loc} + E_{\rm sym}^{\rm mdi},\\
E_{\rm sym}^{\rm kin} &= \frac{1}{\delta^2}\left[\frac{3}{5}\frac{p_{Fn}^2}{2m}\frac{\rho_n}{\rho} + \frac{3}{5}\frac{p_{Fp}^2}{2m}\frac{\rho_p}{\rho} - \frac{3}{5}\frac{p_F^2}{2m}\right]\\
&\approx 12.57\left(\frac{\rho}{\rho_0}\right)^{2/3},\\
E_{\rm sym}^{\rm loc} &= \frac{C_{\rm sp}}{2}\left(\frac{\rho}{\rho_0}\right)^{\gamma_i},\\
E_{\rm sym}^{\rm mdi} &= \frac{1}{\delta^2}\sum_\tau (1+x)\frac{1}{\rho}\iint v(\mathbf{p},\mathbf{p}')f_\tau(\mathbf{r},\mathbf{p})f_\tau(\mathbf{r},\mathbf{p}')d\mathbf{p}d\mathbf{p}'\\
&\quad + \frac{1}{\delta^2}\sum_\tau (1-x)\frac{1}{\rho}\iint v(\mathbf{p},\mathbf{p}')f_\tau(\mathbf{r},\mathbf{p})f_{-\tau}(\mathbf{r},\mathbf{p}')d\mathbf{p}d\mathbf{p}'\\
&\quad - \frac{1}{\delta^2}\frac{1}{\rho}\iint v(\mathbf{p},\mathbf{p}')f(\mathbf{r},\mathbf{p})f(\mathbf{r},\mathbf{p}')d\mathbf{p}d\mathbf{p}'.
\end{aligned} \tag{7}$$

The corresponding slope of the symmetry energy is then

$$L = 3\rho\frac{\partial E_{\rm sym}}{\partial\rho} = 25.14 + \frac{3C_{\rm sp}\gamma_i}{2} + 3\rho\frac{\partial E_{\rm sym}^{\rm mdi}}{\partial\rho}. \tag{8}$$

In order to emphasize the role of the momentum-dependent interaction in the symmetry energy, the momentum-dependent parts of symmetry energies are shown as a function of density in Fig. 5. It can be seen that even though the effective $k$-mass splitting is not taken into account, i.e., $x = 0$, the momentum-dependent interaction contributes to the symmetry energy. The value of $E_{\rm sym}^{\rm mdi}$ for $x = 0$ increases with increasing density. At normal density $\rho_0$, it reaches 5.3 MeV. Actually in the

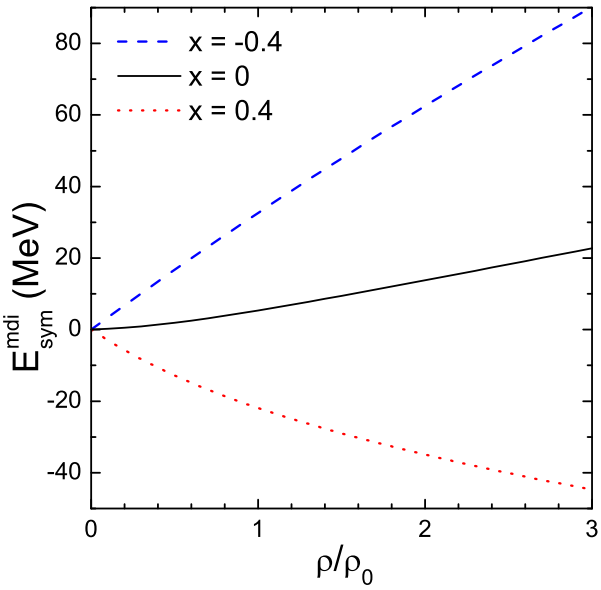


FIG. 5. Momentum-dependent part of symmetry energies as a function of density.

framework of the Brueckner theory or the Hugenholtz–Van Hove (HVH) theorem, the symmetry energy is expressed by two terms (see Eq. (3) in Ref. [40]). One of them depends on the effective $k$ mass and Fermi momentum, and the other depends on the density and Fermi momentum. It is noted that the symmetry energy shown as Eqs. (7) and (8) satisfies the HVH theorem, because the effective $k$ mass, which is related to $v(\mathbf{p},\mathbf{p}')$, has been taken into account.

When the effective $k$-mass splitting is considered, the contribution of momentum-dependent interaction in the symmetry energy is more obvious. In the case of $x = -0.4$, i.e., $m_n^* > m_p^*$ in neutron-rich nuclear, the value of $E_{\rm sym}^{\rm mdi}$ increases with increasing density and reaches 32.6 MeV. For $x = 0.4$, i.e., $m_n^* < m_p^*$, the value of $E_{\rm sym}^{\rm mdi}$ decreases with increasing density and reaches $-21.9$ MeV. It is thus explicit that the symmetry energy and the effective $k$-mass splitting correlate to each other.

In this work, the total symmetry energy depends not only on the parameter $x$ but also on the parameters $C_{\rm sp}$ and $\gamma_i$. The parameters $C_{\rm sp}$ and $\gamma_i$ for a given $x$ are adjusted based on the current constraints on the symmetry energy and its density slope at normal density. So far many analyses have been undertaken attempting to constrain the density dependence of symmetry energy, but divergences still remain. Li and Han [40] have summarized the global averages and standard deviations of $E_{\rm sym}(\rho_0)$ and $L(\rho_0)$ using 28 recent analyses of various terrestrial nuclear laboratory experiments and astrophysical observations. Here, we consider two standard deviations and fit the parameters $C_{\rm sp}$ and $\gamma_i$. Table I shows the four obtained groups of parameters, which provide different density dependences of symmetry energy and effective $k$-mass splittings. Figure 6 shows the corresponding symmetry energy for zero temperature. Both Pos-S and Pos-H parameters provide $m_n^* > m_p^*$ in neutron-rich nuclear matter, but they give soft and hard symmetry energies respectively, as shown

TABLE I. Parameters of symmetry energies and effective $k$-mass splittings.

| | $x$ | $C_{s,p}$ (MeV) | $\gamma_i$ | $E_{\rm sym}(\rho_0)$ (MeV) | $L(\rho_0)$ (MeV) | $m^*$ |
|---|---|---|---|---|---|---|
| Pos-S | $-0.4$ | $-30.87$ | 2.002 | 29.76 | 25.9 | $m_n^* > m_p^*$ |
| Pos-S | $-0.4$ | $-23.51$ | 0.757 | 33.44 | 91.9 | $m_n^* > m_p^*$ |
| Neg-S | 0.4 | 78.21 | 0.408 | 29.76 | 25.9 | $m_n^* < m_p^*$ |
| Neg-H | 0.4 | 85.57 | 0.888 | 33.44 | 91.9 | $m_n^* < m_p^*$ |

in Fig. 6(a). In Fig. 6(b), different density dependences of symmetry energy can also be seen for Neg-S and Neg-H parameters, which provide $m_n^* < m_p^*$ in neutron-rich nuclear matter.

In order to test our parametrization in the transport model, the four groups of parameters of isospin- and momentum-dependent interaction are applied in the IQMD+GEMINI model to calculate the isospin transport ratios obtained from the yield ratios of $A = 7$ isotopes in collisions involving $^{124}$Sn and $^{112}$Sn nuclei at impact parameters of $b = 6$ fm and at 50 MeV/nucleon [34], and the double ratios of the coalescence invariant neutron and proton spectra in central $^{124}$Sn + $^{124}$Sn and $^{112}$Sn + $^{112}$Sn collisions at 50 and 120 MeV/nucleon [33]. In this theoretical framework, the IQMD model is applied to describe the formation of the prefragments, while the GEMINI model [49] is applied to simulate the prefragment decays. The evolution time of IQMD is 500 fm/$c$, since the excited energies of the heavy prefragments are less than 5 MeV/nucleon. Then the GEMINI model is applied. A detailed description of the IQMD+GEMINI model can be found in Ref. [50].

## III. RESULTS

Figure 7 shows the isospin transport ratios as a function of the rapidity. Data shown as solid circles are taken from

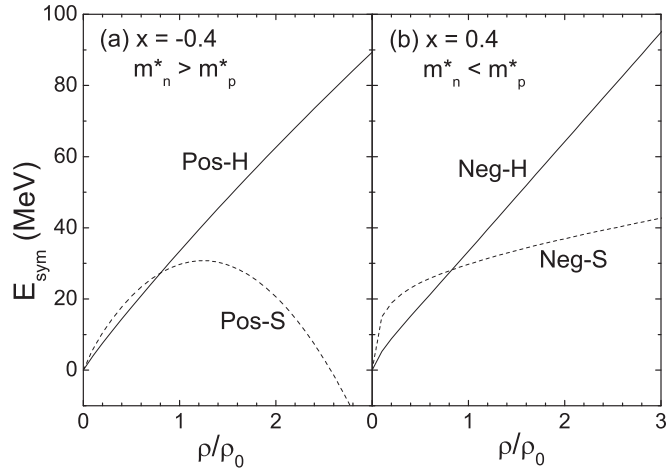


FIG. 6. Symmetry energies as a function of density within (a) Pos-S and Pos-H parameters which provide $m_n^* > m_p^*$ in neutron-rich nuclear matter, (b) Neg-S and Neg-H parameters which provide $m_n^* < m_p^*$ in neutron-rich nuclear matter.

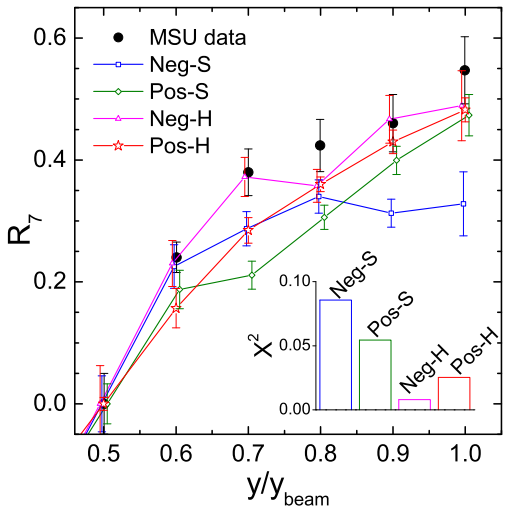


FIG. 7. Isospin transport ratios obtained from the yield ratios of $A = 7$ isotopes in collisions involving $^{124}$Sn and $^{112}$Sn nuclei at impact parameters of $b = 6$ fm and at 50 MeV/nucleon. Data shown as solid circles are taken from Ref. [34]. The inside panel shows the total square $X^2$ computed from the difference between data and calculations.

Ref. [34]. The calculations are obtain from 10 000 000 simulated events. The computation uncertainties are statistical. Despite the large uncertainties, it is shown that the calculations for Neg-H are the closest to the data. The inset shows the total square $X^2$ computed from the difference between data and calculations for four groups of interactions. One can see that the total squares $X^2$ for Neg-H and Pos-H are smaller than in the other two cases. That is, whether $m_n^* < m_p^*$ or $m_n^* > m_p^*$, the hard symmetry energies with $E_{\rm sym}(\rho_0) = 33.44$ MeV and $L(\rho_0) = 91.9$ reproduce the data better than the soft symmetry energies with $E_{\rm sym}(\rho_0) = 29.76$ MeV and $L(\rho_0) = 25.9$. This phenomenon supports the deduction in Ref. [42] that the isospin diffusion observable is sensitive to the symmetry energy rather than the effective $k$-mass splitting.

Figure 8 shows the double ratios in the upper panel for 50 MeV/nucleon and bottom panel for 120 MeV/nucleon. Comparing the dashed line and dash-dotted line, one can see that the calculations with Neg-S ($m_n^* < m_p^*$) are larger than those with Pos-S ($m_n^* > m_p^*$). Note that both Neg-S and Pos-S parameters provide soft symmetry energies with $E_{\rm sym}(\rho_0) = 29.76$ MeV and $L(\rho_0) = 25.9$. When the hard symmetry energies with $E_{\rm sym}(\rho_0) = 33.44$ MeV and $L(\rho_0) = 91.9$ are considered, it also indicates that $m_n^* < m_p^*$ leads to a larger value of double ratios than $m_n^* > m_p^*$. This deduction has been obtained in Refs. [32,33]. Significantly the calculations within Neg-S parameters are obviously larger than those within Neg-H parameters, even though the effective $k$-mass splittings for both parameters are the same. In other words, the effects of local symmetry energy and effective $k$-mass splitting on the double ratios are synchronous.

It has been proposed that there are two competing effects of symmetry energy on the double ratios [34]. Specifically, higher symmetry energy at subnormal density enhances the emission of neutrons, resulting in larger double ratios, but too high symmetry energy will result in the system completely

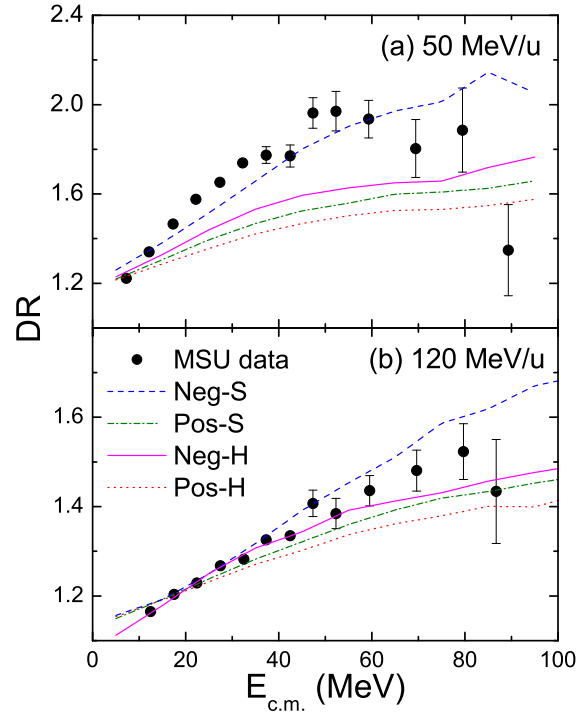


FIG. 8. Double ratios of the coalescence invariant neutron and proton spectra in central $^{124}$Sn+$^{124}$Sn and $^{112}$Sn+$^{112}$Sn collisions at (a) 50 and (b) 120 MeV/nucleon. Calculations within different parameters are shown as lines. Data shown as solid circles are taken from Ref. [33].

disintegrating, reducing the double ratios to the limit $\frac{N/Z(^{124}\rm Sn)}{N/Z(^{112}\rm Sn)}$. The physical condition may be more complex, because the total symmetry energy includes three components: i.e., the kinetic symmetry energy, the local potential symmetry energy, and the momentum-dependent symmetry energy. Here, the momentum-dependent symmetry energy depends on the effective $k$-masses splitting. Not only the total symmetry energy but also each component affects the double ratios. It has been found that lower kinetic symmetry energies yield larger values of the double ratios [38,39]. Our calculations, together with those in Refs. [32,33], certify the fact that the negative value of $m_n^* - m_p^*$ leads to larger value of double ratios than positive $m_n^* - m_p^*$. In addition, our calculations indicate the strong effects of local symmetry energy on the double ratios.

## IV. CONCLUSION

In conclusion, the isospin- and momentum-dependent interaction used in IQMD model is extracted. The momentum dependence of the interaction is fitted to the optical potentials extracted with proton-nucleus scattering data, while the isospin dependence is adjusted based on the current constraints on the symmetry energy and their density slope at normal density. The nucleon effective mass as a function of momentum is calculated and compared with results from the DBHF model. The calculations using the DBHF model show that the nonlocality in space results in a smooth increase of effective masses with increasing momenta, while the nonlocality in

time results in a peak and valley above the Fermi momentum [11]. Our parametrization can reproduce the calculations of the DBHF model without considering the nonlocality in time. After considering the effective $k$-mass splitting, the total symmetry energy is composed of the kinetic symmetry energy, the local potential symmetry energy, and the momentum-dependent symmetry energy. It is shown that the contribution of the momentum-dependent interaction in the symmetry energy is obvious. The current constraints on the total symmetry energy can accommodate a wide-range adjustment of the local symmetry energy and effective $k$-mass splitting.

Four groups of parameters, which provide different density dependences of symmetry energies and effective $k$-mass splittings, are applied in the IQMD+GEMINI model to calculate the isospin diffusion and neutron-to-proton double ratios in collisions involving $^{124}$Sn and $^{112}$Sn nuclei at 50 and 120 MeV/nucleon. It is found that the isospin diffusion observable is sensitive to the symmetry energy rather than the effective $k$-mass splitting. The negative value of $m_n^* - m_p^*$ leads to larger value of double ratios than positive $m_n^* - m_p^*$. However, the effect of the local symmetry energy on the double ratios exists synchronously. It is proposed that the uncertainty of the symmetry energy is necessary to be considered if one wishes to constrain the effective $k$-mass splitting by double ratio data.

## ACKNOWLEDGMENTS

This work was supported by the National Natural Science Foundation of China under Grants No. 11405278, No. 11505150, and No. 11161130520, the Fundamental Research Funds for the Central Universities under Grant No. 15lgpy30, the Natural Science Foundation of Guangdong Province China under Grant No. 2016A030310208, the Yuncheng University Research Project under Grant No. YQ-2014014, and the China Postdoctoral Science Foundation under Grant No. 2015M582730.

[1] N. Bohr, Nature (London) **137**, 344 (1936).
[2] P. Danielewicz, R. Lacey, and W. G. Lynch, Science **298**, 1592 (2002).
[3] C. Fuchs and H. H. Wolter, Eur. Phys. J. A **30**, 5 (2006).
[4] G. Giuliani, H. Zheng, and A. Bonasera, Prog. Part. Nucl. Phys. **76**, 116 (2014).
[5] A. W. Steiner, M. Prakash, J. M. Lattimer, and P. J. Ellis, Phys. Rep. **411**, 325 (2005).
[6] B. A. Li, L. W. Chen, and C. M. Ko, Phys. Rep. **464**, 113 (2008).
[7] V. Baran, M. Colonna, V. Greco, and M. Di Toroa, Phys. Rep. **410**, 335 (2008).
[8] L. L. Li, Z. H. Li, E. G. Zhao, S. G. Zhou, W. Zuo, A. Bonaccorso, and U. Lombardo, Phys. Rev. C **80**, 064607 (2009).
[9] Q. B. Shen, Y. L. Han, and H. R. Guo, Phys. Rev. C **80**, 024604 (2009).
[10] J. Xu, Phys. Rev. C **91**, 037601 (2015).
[11] M. Jaminon and C. Mahaux, Phys. Rev. C **40**, 354 (1989).
[12] E. N. E. van Dalen, C. Fuchs, and A. Faessler, Phys. Rev. Lett. **95**, 022302 (2005).
[13] W. Zuo, L. G. Cao, B. A. Li, U. Lombardo, and C. W. Shen, Phys. Rev. C **72**, 014005 (2005).
[14] H. F. Zhang, Z. H. Li, U. Lombardo, P. Y. Luo, F. Sammarruca, and W. Zuo, Phys. Rev. C **76**, 054001 (2007).
[15] F. Sammarruca, Int. J. Mod. Phys. E **19**, 1259 (2010).
[16] L. Ou, Z. X. Li, Y. X. Zhang, and M. Liu, Phys. Lett. B **697**, 246 (2011).
[17] L. W. Chen, C. M. Ko, and B. A. Li, Phys. Rev. C **76**, 054316 (2007).
[18] L. G. Arnold, B. C. Clark, E. D. Cooper, H. S. Sherif, D. A. Hutcheon, P. Kitching, J. M. Cameron, R. P. Liljestrand, R. N. MacDonald, W. J. McDonald, C. A. Miller, G. C. Neilson, W. C. Olsen, D. M. Sheppard, G. M. Stinson, D. K. McDaniels, J. R. Tinsley, R. L. Mercer, L. W. Swensen, P. Schwandt, and C. E. Stronach, Phys. Rev. C **25**, 936 (1982).
[19] S. Hama, B. C. Clark, E. D. Cooper, H. S. Sherif, and R. L. Mercer, Phys. Rev. C **41**, 2737 (1990).
[20] E. D. Cooper, S. Hama, B. C. Clark, and R. L. Mercer, Phys. Rev. C **47**, 297 (1993).
[21] C. Hartnack and J. Aichelin, Phys. Rev. C **49**, 2801 (1994).
[22] J. Aichelin, A. Rosenhauer, G. Peilert, H. Stoecker, and W. Greiner, Phys. Rev. Lett. **58**, 1926 (1987).
[23] J. Xu, L. W. Chen, and B. A. Li, Phys. Rev. C **91**, 014611 (2015).
[24] M. Prakash, J. Wambach, and Z. Y. Ma, Phys. Lett. B **128**, 141 (1983).
[25] S. Shlomo and J. B. Natowitz, Phys. Lett. B **252**, 187 (1983).
[26] C. B. Das, S. Das Gupta, C. Gale, and B. A. Li, Phys. Rev. C **67**, 034611 (2003).
[27] Ch. C. Moustakidis, Phys. Rev. C **78**, 054323 (2008).
[28] J. W. Negele and K. Yazaki, Phys. Rev. Lett. **47**, 71 (1981).
[29] J. Rizzo, M. Colonna, M. Di Toro, and V. Greco, Nucl. Phys. A **732**, 202 (2004).
[30] C. Xu, B. A. Li, and L. W. Chen, Phys. Rev. C **82**, 054607 (2010).
[31] W. J. Xie and F. S. Zhang, Phys. Lett. B **735**, 250 (2014).
[32] Y. X. Zhang, M. B. Tsang, Z. X. Li, and H. Liu, Phys. Lett. B **732**, 186 (2014).
[33] D. D. S. Coupland, M. Youngs, W. G. Lynch, M. B. Tsang, Z. Chajecki, Y. X. Zhang, M. A. Famiano, T. K. Ghosh, B. Giacherio, M. A. Kilburn, J. Lee, F. Lu, P. Russotto, A. Sanetullaev, R. H. Showalter, G. Verde, and J. Winkelbauer, Phys. Rev. C **94**, 011601(R) (2016).
[34] M. B. Tsang, Y. X. Zhang, P. Danielewicz, M. Famiano, Z. X. Li, W. G. Lynch, and A. W. Steiner, Phys. Rev. Lett. **102**, 122701 (2009).
[35] Z. Y. Sun, M. B. Tsang, W. G. Lynch, G. Verde, F. Amorini, L. Andronenko, M. Andronenko, G. Cardella, M. Chatterje, P. Danielewicz, E. De Filippo, P. Dinh, E. Galichet, E. Geraci, H. Hua, E. La Guidara, G. Lanzalone, H. Liu, F. Lu, S. Lukyanov, C. Maiolino, A. Pagano, S. Piantelli, M. Papa, S. Pirrone, G. Politi, F. Porto, F. Rizzo, P. Russotto, D. Santonocito, and Y. X. Zhang, Phys. Rev. C **82**, 051603 (2010).
[36] L. W. Chen, C. M. Ko, and B. A. Li, Phys. Rev. Lett. **94**, 032701 (2005).
[37] H. Y. Kong, Y. Xia, J. Xu, L. W. Chen, B. A. Li, and Y. G. Ma, Phys. Rev. C **91**, 047601 (2015).

[38] O. Hen, B. A. Li, W. J. Guo, L. B. Weinstein, and E. Piasetzky, Phys. Rev. C **91**, 025803 (2015).
[39] B. A. Li, W. J. Guo, and Z. Z. Shi, Phys. Rev. C **91**, 044601 (2015).
[40] B. A. Li and X. Han, Phys. Lett. B **727**, 276 (2013).
[41] X. H. Li, W. J. Guo, B. A. Li, L. W. Chen, F. J. Fattoyev, and W. G. Newton, Phys. Lett. B **743**, 408 (2015).
[42] Y. X. Zhang, M. B. Tsang, Z. X. Li, F. J. Fattoyev, and W. G. Newton, Phys. Lett. B **749**, 262 (2015).
[43] J. Aichelin, Phys. Rep. **202**, 233 (1991).
[44] G. M. Welke, M. Prakash, T. T. S. Kuo, S. DasGupta, and C. Gale, Phys. Rev. C **38**, 2101 (1988).
[45] T. Gaitanos, M. Kaskulov, and U. Mosel, Nucl. Phys. A **828**, 9 (2009).
[46] S. Typel, O. Riedl, and H. H. Wolter, Nucl. Phys. A **709**, 299 (2002).
[47] B. ter Haar and R. Malfliet, Phys. Rep. **149**, 207 (1987).
[48] A. Ono and J. Randrup, Eur. Phys. J. A **30**, 109 (2006).
[49] R. J. Charity, M. A. McMahan, G. J. Wozniak, R. J. McDonald, L. G. Moretto, D. G. Sarantites, L. G. Sobotka, G. Guarino, A. Pantaleo, L. Fiore, A. Gobbi, and K. D. Hildenbrand, Nucl. Phys. A **483**, 371 (1988).
[50] J. Su, K. Cherevko, W. J. Xie, and F. S. Zhang, Phys. Rev. C **89**, 014619 (2014).